ACS OMEGA

http://pubs.acs.org/journal/acsodf

Article

Lyotropic Liquid Crystal-Based Membranes for Water Remediation: Fabrication, Characterization and Performance Evaluation

Liz Santiago-Martoral, Adrialis Figueroa, and Eduardo Nicolau*

Cite This: *ACS Omega* 2020, 5, 17940−17946

Read Online

ACCESS | Metrics & More | Article Recommendations | Supporting Information

ABSTRACT: In water remediation, biomimetic membranes are gaining much attention due to their selectivity, dynamic stability, nontoxicity, and biocompatibility. Lyotropic liquid crystals (LLCs) are self-organizing networks that can conform to an array of geometries with high pore densities. As such, LLCs are excellent membrane materials for water applications because they are water insoluble and are manipulated to conform to an array of morphologies that provide natural water channels that are readily tunable in size. They have the ability to create uniform pores, between the range of 1 and 5 nm, with large surface areas. Thus, this work focuses on the design, fabrication, and characterization of LLC-modified Janus-type membranes for forward osmosis applications. Physical characterization of the membranes was performed using scanning electron microscopy (SEM), and the results show an open-pore radius and the presence of both finger- and sponge-like pores depending on membrane preparation. The contact angle assessment indicates that as the membranes are further modified with other polymers (e.g., PAN), higher hydrophilicity and surface energy are achieved. Moreover, the Brunauer−Emmett−Teller (BET) analysis showed a significant variation in the pore distribution between membranes. Functionalized membranes presented satisfactory water flux and superior salt rejection compared to nonfunctionalized membranes. SupPACMoDS membranes are 83% more efficient at preventing salt back flux than the nonmodified version. This is credited to the thickness and pore structure provided by the PAN support layer in the membrane.

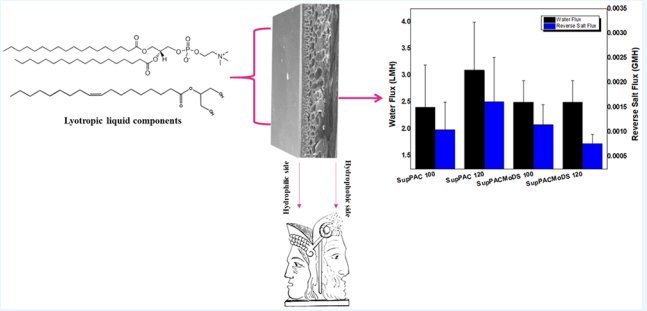

1. INTRODUCTION

The human and industrial overuse of water resources is creating a strain on our natural resources. As such, water is becoming scarce, and it is expected to become the target for conflicts due to its high demand and reduced availability.[1] Water reclamation is of notable significance in developing countries, where the supply and access to clean water are quite limited.[2] Current water filtration strategies are geared toward reclaiming water with the use of membrane-based processes. In water reclamation applications, some of the most common membrane processes are ultrafiltration (UF) and reverse osmosis (RO).[2−4] Although both of these technologies have been proven to be effective, the use of high pressure as a driving force to promote water flux is not ideal since high external energy inputs are required and methods are not cost-effective.[4]

In contrast, forward osmosis (FO) is a membrane-based process that becomes an asset due to its minimum power consumption; in FO, the flux is generated when a concentrated draw solution creates a high osmotic pressure, which pulls water across a semipermeable membrane from the feed solution.[3] FO is a passive process in terms of energy input, and therefore, membranes are prone to the effects of a low-pressure differential across the membrane. Some of the challenges of FO are contaminant permeation, membrane fouling, and high pretreatment costs. To help address these challenges, researchers in this field have proposed several strategies, such as multiblock copolymers, carbon nanotubes, polymerizable surfactants, and biomimetic membranes.[5−9]

Biomimetic membranes have gained significant interest due to their higher water flux, solute rejection, and environmental sustainability when compared to available commercial membranes.[10,11] Processes and materials related to biomimicry are gaining interest in the commercialization for water treatment applications, such as FO. Currently, they demonstrate a set of enhancements that are based on robustness, water permeability, solute selectivity, cost, and compatibility.[10,12,13] Even though biomimetic membranes have commercial limitations, they show significant potential for efficiency improvement.[13] Therefore, by incorporating nanocomposite-

Received: March 2, 2020
Accepted: July 2, 2020
Published: July 20, 2020

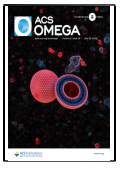

https://dx.doi.org/10.1021/acsomega.0c00946
ACS Omega 2020, 5, 17940−17946

based membranes, they provide an opportunity for further modifications and performance enhancements.[14,15]

A strategy that is still under development is the use of nonlamellar lyotropic liquid crystals (LLCs) as the selective layer in thin-film composite membranes. Previously, LLCs have been extensively studied for drug delivery purposes and for their use as semiconducting materials.[16−21] Nonlamellar lyotropic liquid crystals are an exciting and promising class of materials that may prove useful to fabricate the next generation of biomimetic membranes.[22−24] LLCs are nanocompartmentalized biomaterials that can self-assemble in aqueous media and create built-in ordered nanosized pores. These materials can self-assemble into various geometries such as two-/three-dimensional forms, hexagonal, or bicontinuous cubic.[24−26]

The driving force for the self-assembly is the hydrophobic effect caused by carbon tails to minimize interactions with water.[27] The head groups of the lipids used in the mixture sustain the layer conformation with variation in the packing density.[28] In membrane development, these materials are advantageous because they provide thermodynamic stability, are biocompatible, and are highly stable in excess water.[29,30] Membranes incorporated with LLCs show great filtration performance and ion selectivity such as the one previously published by Henmi, Nada, and Hamaguchi.[31−33]

In addition, since the membranes undergo surface modification, the resulting modified membranes have Janus membrane properties. The name Janus comes from the two-faced Roman god; therefore, Janus membranes have two sides with varying properties: one side is hydrophobic and the other, hydrophilic.[34] Janus materials are gaining popularity and show promise due to their properties such as selective transport, antiwetting properties, and fluid transport manipulation among other features.[35−37] This article focuses on the development of an LLC-based Janus-type membrane composed of a phosphatidylcholine called 1,2-distearoyl-*sn*-glycero-3-phosphocholine (DSPC) and monoolein (Mo). Monoolein is a glycerol lipid that is already well known to form highly organized LLC structures.[27,38−40] This mixture is assessed to understand further the feasibility of a membrane with a variation in the monomer composition and provide insight into the viability of future composition variations.

2. RESULTS AND DISCUSSION

2.1. Membrane Characterization. A membrane support structure should be biologically, mechanically, and thermally stable. Therefore, SEM provides insight into the porous structure of the membrane and provides a visual explanation for a nondimensional indication permeability that is given by the aspect ratio of the pore geometry; hence, we evaluate pore structures with SEM images for the unmodified membrane SupP and modified membranes SupPAC and SupPACMoDS. The membranes prepared at a PAN casting solution thickness of 100 μm are shown in Figure 1. There is apparent smoothness in the surface of the active layer of the membrane, and surface modification occurs. The transversal cut images show a noticeable variation in the pore size and type. For the SupP membrane, there are defined finger-like pores; for SupPAC and SupPACMoDS, the finger-like pores shorten, and large sponge-like pores appear. In the case of SupPACMoDS, this might be caused by heating when the membrane is modified with NaOH, and when the LLCs are added.

To further understand these effects, BET analysis was performed to approximate the pore size and surface area of the

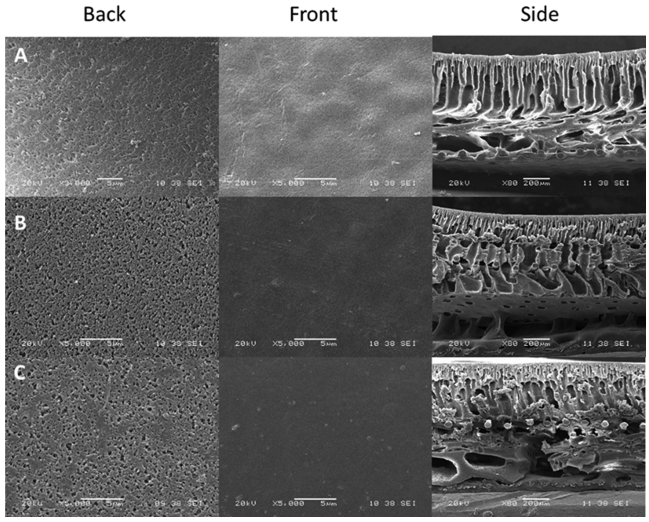

Figure 1. SEM images of membranes with a 100 μm PAN casting solution thickness. The images show the back, front, and cross-sections for (a) SupP, (b) SupPAC 100, and (c) SupPACMoDS 100.

100 μm membranes, see Figure 2. The BET technique is becoming useful for membrane characterization as it provides direct information of the porosity and allow to predict the eventual transport of molecules.[41−43] Gas adsorption techniques are useful when determining the porosity and pore surface area compared to other techniques. As can be established from the results, when the membrane is modified, there is an increased surface area, although the pore size is not proportional. Two samples for each membrane were evaluated. Since the unmodified SupP has the lowest BET surface area and modifications of the micropore surface area take place, these two variables increase. The pore size for SupPAC is smaller than those for SupP and SupPACMoDS, and this can be attributed to the cavities formed by the polyionic layer that, with the pressure exerted, promoted a collapsed state.[44] The isotherm for the SupP and SupPAC membranes resembles type III isotherm, indicating a multilayer formation process where typically the adsorbate−adsorbent interactions are low.[45,46] SupPACMoDS shows a type V isotherm; it is similar to type III due to low adsorbate−adsorbent interactions. However, type V has a present hysteresis loop that can be attributed to cavitation-induced evaporation or percolation in narrow pore necks. The pore size is likely to be associated with the hexagonal water channel with a diameter of ∼ 5 nm, as has been previously reported.[25,47−49]

Furthermore, the SEM images of the membrane with a PAN casting solution thickness of 120 μm are shown in Figure 3. As can be observed from these images, the SupP membrane (Figure 3a) shows small but wide and defined finger-like pores. Similarly, the SupPAC membrane (Figure 3b) presents long and defined finger-like pores that stretch through the entire membrane material. Once again, the SupPACMoDS membrane (Figure 3c) presents a combination of pores; it has small finger-like pores and larger sponge-like pores. This confirms that the heating process does affect the pore structure of the PAN-supported membrane.

Here is an increment in the pore size as modification takes place compared to 100 μm. The isotherm graph shows a type IV isotherm, which is typical for mesoporous solids, where the solid gets absorbed in a multilayer manner.[45,50] Moreover, this type of isotherm is associated with capillary condensation,

https://dx.doi.org/10.1021/acsomega.0c00946
ACS Omega 2020, 5, 17940−17946

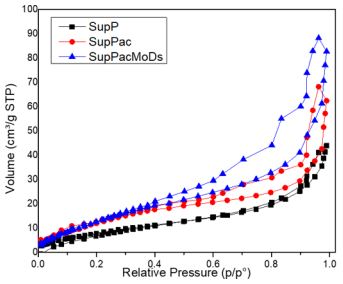

	SupP	Sup-PAC	SupPACMoDs
BET Surface Area	32 m²/g	56 m²/g	60 m²/g
Pore Size (average)	4.6 nm	4.3 nm	4.8 nm
Micropore surface area	24 m²/g	41 m²/g	49 m²/g

Figure 2. BET isotherms for 100 μm SupP, SupPAC, and SupPACMoDS membranes to determine the pore size and surface area and tabulated values.

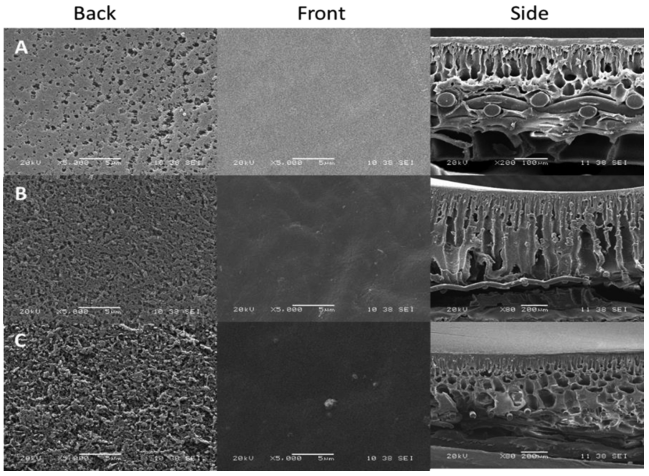

Figure 3. SEM images of membranes with a 120 μm PAN casting solution thickness. The images show the back, front, and cross-sections for (a) SupP, (b) SupPAC 120, and (c) SupPACMoDS 120.

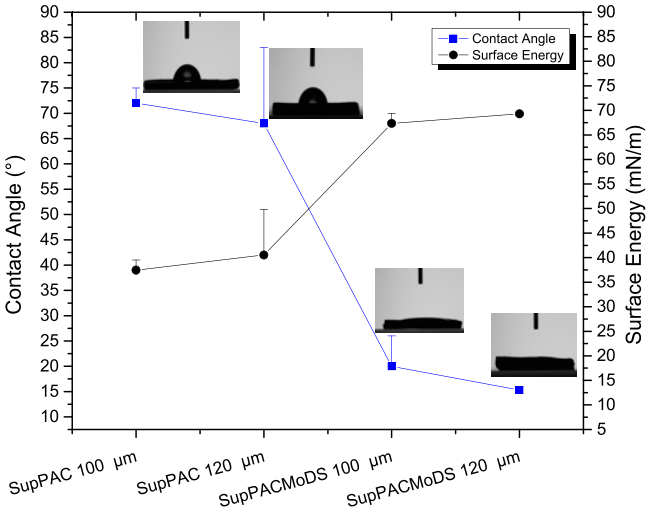

Figure 5. Contact angle and surface energy results with contact angle images after 60 s for 100 and 120 μm membranes.

which takes place within the pores due to increased van der Waals interactions and is the theoretical limit of adsorption stability.[51,52] This occurs when the pore width exceeds a certain critical width, which is dependent on the adsorption system and temperature. The capillary condensation can be associated with large pore channels that can be confirmed with the SEM images. BET analysis was also used to approximate the pore size and surface area of the 120 μm membranes (Figure 4).[23,53]

As a strategy to understand the surface free energy aspects of the fabricated membranes, the contact angle technique was employed to determine the hydrophilicity/hydrophobicity of the membranes (Figure 5).[54−56] The SupPAC membranes have a high contact angle and low surface energy; these indicate weaker attractive forces between the material surface and the water droplet. The results suggest that adding the polyanion and polycation layers creates a disturbance in the surface energy and promotes partial nonwetting.[57,58] Moreover, the LLC surface promotes complete wetting on the surface, which can be attributed to the exposed polar side of the LLC mixture.

SupPAC 120 exhibits a contact angle of 68° and a surface energy of 42 mN/m and SupPAC 100 shows a contact angle of 72° and a surface energy of 39 mN/m, whereas SupPACMoDS 100 shows a contact angle of 20° and a surface energy of 68 mN/m. The SupPACMoDS membranes present a much lower contact angle and much stronger attractive forces, hinting at better permeability. However, SupPAC 120 and SupPACMoDS 120 have slightly lower contact angle values than their counterparts. These results are not only due to the membrane

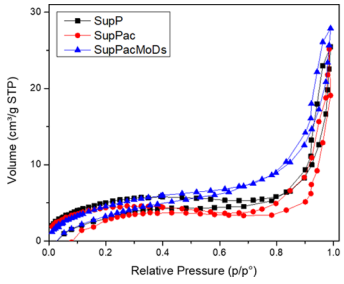

	SupP	Sup-PAC	SupPACMoDs
BET Surface Area	20 m²/g	16 m²/g	19 m²/g
Pore Size (average)	5.1 nm	5.7 nm	5.6 nm
Micropore surface area	13 m²/g	13 m²/g	20 m²/g

Figure 4. BET isotherms for 120 μm-thick SupP, SupPAC, and SupPACMoDS membranes to determine the pore size and surface area and tabulated values.

https://dx.doi.org/10.1021/acsomega.0c00946
ACS Omega 2020, 5, 17940−17946

surface chemical composition but also due to their more organized pore arrangement since the morphology of the pores contributes, as previously observed in SEM. The 120 μm SupPACMoDS membrane shows a contact angle of 15° and a surface energy of 70 mN/m, indicating that this membrane has higher hydrophilicity and favors permeation.

To determine whether this behavior correlates with membranes with higher water permeation, an FO test was performed on each membrane. An ideal FO membrane is the one that has high water flux and low reverse salt flux. The parameters that were considered were water flux (J_w) and reverse salt flux (J_s) and the errors were all less than 1 LMH for water flux and less than 0.001 for reverse salt flux. SupPAC 120 showed the highest water flux of 3.1 LMH; this is linked to the directionality and size of the pore previously determined by BET analysis and observed by SEM. The error bars indicate the preciseness of the measurements; therefore, a smaller error indicates fewer deviations between runs. In the case of SupPAC 120, the membrane has a higher water flux, but error bars signify a considerable deviation between runs.

Moreover, an exposed charged layer combined with an increased water flux might be responsible for a higher reverse salt value. In the case of the modified SupPAC MoDS100 and 120, they both provide the same water flux, 2.5 LMH, but the reverse salt flux, which indicates that the salt rejection was optimal for SupPAC MoDS120, suggesting that the membrane thickness combined with the LLC modification has a positive effect on limiting reverse salt diffusion (Figure 6). SupPACMoDS 120 emerges as the most feasible membrane for this application due to a much lower reverse salt flux and beneficial water flux.[59]

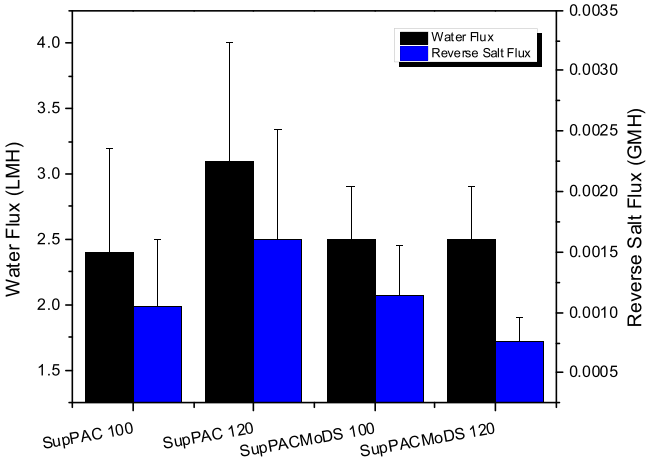

Figure 6. Water and reverse salt flux results of membranes exposed to the FO bench-scale FO system.

3. CONCLUSIONS

In summary, this work dealt with the fabrication, characterization, and performance evaluation of a new class of water purification membranes with an LLC layer. This alteration provides a feasible membrane for forward osmosis that has acceptable water flux and enhanced salt rejection properties. In addition, the biomimetic membrane BET characterization provides insights into the LLC structure and possible pore modifications that can be performed to enhance the properties of the membrane further. The designed biomimetic membrane has the potential to be employed for wastewater reclamation, drug extraction, emerging contaminant, and small contaminant entrapment and degradation.

4. EXPERIMENTAL SECTION

4.1. Materials. Monoolein (MO) unsaturated was purchased from Fisher Scientific (USA). Phosphate-buffered saline 1 M, pH 7.4, and the photoinitiator hydroxy-2-methylpropiophenone were purchased from Sigma (USA); 1,2-Distearoyl-*sn*-glycero-3-phosphocholine (DSPC) (1 g) was purchased from Fischer Scientific (USA). Polyethyleneimine branched (PEI, Mw ~ 25,000), poly(sodium 4-styrenesulfonate) (PSS, Mw ~ 70,000) powder, polyacrylonitrile (PAN, Mw ~ 150,000), and dimethyl sulfoxide (purity = 99.5%) were purchased from Sigma Aldrich. Polyester Mesh 105 Micron-Open Area %: 52—Width: 40 in. was purchased from Elko Filtering CO. Sodium chloride (NaCl, ACS reagent > 99%) was purchased from Sigma Aldrich. Milli Q water with a resistivity of 18.23 MΩ·cm^2 was used at all times.

4.2. Methods. *4.2.1. Membrane Preparation.* Polyacrylonitrile-based membranes were prepared using 12% DMSO with 2% LiCl at 60 °C overnight.[41] Then, the solution was cast on a polyester mesh and the porous membrane substrate was prepared by the phase inversion method; these membranes are labeled as SupP. In the aforementioned process, two PAN solution thicknesses were prepared at 100 and 120 μm to examine how varying PAN thickness affected the membrane performance and properties. The PAN membrane was exposed and immersed in a NaOH 1.5 M solution at 45 °C for 1.5 h. After the membranes were rinsed with nanopure water, the PEI (1 %w/v) prepared in aqueous solution was added to the top layer. After rinsing with nanopure water, 1%w/v PSS was prepared in aqueous solution. The PEI was deposited on top of the PAN membrane to form a polycation layer, whereas the PSS solution was deposited to form the polyanion layer, and both were added to promote stability and adherence from the zwitterionic phosphocholine to the membrane support. Each deposition had a duration time of 30 min, and each absorption was followed by a rinse of DI water for approximately 2 min to ensure the removal of redundant polyelectrolytes.[41−43] Membranes following this surface medication are labeled as SupPAC.

4.2.2. Preparation of LLCs and Substrate Deposition. The lipid mixture was first prepared by weighing a certain amount of MO:DSPC (MoDs) at a ratio of 90:10 dissolved in a mixture of chloroform/methanol (200 μL) to obtain a homogenous solution. Then, the bulk of organic solvent was removed by exposing the solution to a gentle stream of nitrogen gas, ensuring that the vial is kept warm to facilitate the process. Afterward, the vials were placed openly under vacuum overnight to ensure that all the traces of the solvent had been removed, and then the lipid mixture was stored at −20 °C. The liquid crystal phase was then prepared using a previously established protocol to obtain the crystalline phase; the mixture was first carefully melted and loaded into a 250 μL Hamilton gas-tight syringe and the aqueous phase in a 100 μL Hamilton gas-tight syringe and the photoinitiator was added at 5% of the total volume, and then they were connected using a syringe coupler, and upon applying mechanical pressure, a clear LLC gel was produced.[44,45] After the LLC was prepared, it was deposited onto a SupPAC membrane. The process requires spreading of the gel on the SupPAC support, by adding the gel onto the membrane and then placing the

https://dx.doi.org/10.1021/acsomega.0c00946
ACS Omega 2020, 5, 17940−17946

membrane in between Mylar sheets and fixing it between two glass plates. The subsequent process involved spreading of the gel to generate a thin gel film. Then, the glass plates were covered with aluminum and placed at 65 °C while being irradiated with UV light at 365 nm for 30 min to promote crosslinking.[46,47] The membranes undergoing this surface modification are labeled as SupPACMoDS.

4.3. Membrane Characterization. *4.3.1. Scanning Electron Microscope.* SEM imaging was conducted using a JEOL 6480LV scanning electron microscope (SEM); for transversal images, the samples were dipped in liquid and cut using a sharp blade, and all samples were placed in sample holders and sputtered with a thin gold film (ca. 10 nm thick).

4.3.2. Brunauer–Emmett–Teller (BET). BET measurements were conducted using a TriStar II 3020, and isotherms were determined using N_2 adsorption at 77.3 K bath temperature. Before the BET measurements, the samples were dried at 40 °C for 1 h.

4.3.3. Contact Angle (CA). The wettability of the SupPAC and SupPACMoDS membranes was evaluated using a Krüss drop shape analyzer DSA25S (Krüss Optronic, Hamburg, Germany) at room temperature. The membranes were cut to obtain 1.5 cm^2 pieces that were fixed to the stage using carbon tape. A 4.25 μL nanopure water droplet was released from a syringe with a 25-gauge flat needle (0.51 mm inner diameter, 0.26 mm outer diameter) onto the surface of the sample. The images of the drop were recorded every 0.5 s up to 60 s and analyzed in real time using the Advance software (version 1.8), and all evaluations were performed in triplicate.

4.4. Forward Osmosis Evaluations. Membrane performance was evaluated using an in-house FO system using nanopure water (18 MΩ·cm^2) as the feed solution and 5 %w/v NaCl as the draw solution. A rectangular piece of the membrane of 2 1/2 × 5 cm was correctly placed in an acrylic FO cell with a membrane active area of 4.25 cm^2, and the active layer was facing the feed solution. All operation conditions were set following a previously published method. FO evaluation was executed by creating a water flux from the feed solution (FS, low osmotic concentration) to the draw solution (DS, high osmotic concentration) by virtue of the osmotic pressure generated. The water flux rate for all membranes was determined using the following equation:

$$J_w = \frac{\Delta V}{A_M t}$$

where J_w is the water flux rate in LMH ($L{\cdot}m^{-2}{\cdot}h^{-1}$), ΔV is the volume increment in the osmotic solution in L, A_M is the active membrane area, and t is the time or the duration of the test in hours (run for 1 h). The reverse salt flux from the draw solution to the feed side was obtained using the following equation:

$$J_s = \frac{\Delta(C_t V_t)}{A_M t}$$

where J_s is the reverse salt flux in GMH ($g{\cdot}m^{-2}{\cdot}h^{-1}$) and C_t and V_t are the salt concentration and the feed volume at the end of the run, respectively. It is important to establish that this process is repeated for a total of $n = 9$ per membrane.

■ ASSOCIATED CONTENT

Supporting Information

The Supporting Information is available free of charge at https://pubs.acs.org/doi/10.1021/acsomega.0c00946.

FTIR and contact angle analyses of modified membranes (PDF)

■ AUTHOR INFORMATION

Corresponding Author

Eduardo Nicolau − *Department of Chemistry and Molecular Sciences Research Center, University of Puerto Rico, San Juan, Puerto Rico 00925-2537, United States;* orcid.org/0000-0002-6116-029X; Phone: 787-292-9820; Email: eduardo.nicolau@upr.edu; Fax: 787-522-2150

Authors

Liz Santiago-Martoral − *Department of Chemistry and Molecular Sciences Research Center, University of Puerto Rico, San Juan, Puerto Rico 00925-2537, United States*

Adrialis Figueroa − *Department of Chemistry and Molecular Sciences Research Center, University of Puerto Rico, San Juan, Puerto Rico 00925-2537, United States*

Complete contact information is available at: https://pubs.acs.org/10.1021/acsomega.0c00946

Author Contributions

The manuscript was written through the contributions of all authors. All authors have given approval to the final version of the manuscript. LSM is the main author of this work.

Notes

The authors declare no competing financial interest.

■ ACKNOWLEDGMENTS

This work was possible due to the funding from the NASA MIRO-Puerto Rico Space Partnership for Research, Education and Training (PR-SPRInT) under grant # 80NSSC19M0236, NASA Experimental Program to Stimulate Competitive Research (EPSCoR) under grant #NNX14AN18A, and the PR NASA Space Grant under grant number NNX15AI11H. The authors acknowledge the UPR Materials Characterization Center (MCC) for providing support during the progress of this work.

■ REFERENCES

(1) Donlan, R. M. Biofilms: microbial life on surfaces. *Emerg. Infect. Dis.* **2002**, *8*, 881.

(2) Warsinger, D. M.; Chakraborty, S.; Tow, E. W.; Plumlee, M. H.; Bellona, C.; Loutatidou, S.; Karimi, L.; Mikelonis, A. M.; Achilli, A.; Ghassemi, A.; Padhye, L. P.; Snyder, S. A.; Curcio, S.; Vecitis, C. D.; Arafat, H. A.; Lienhard V, J. H. A review of polymeric membranes and processes for potable water reuse. *Prog. Polym. Sci.* **2018**, *81*, 209–237.

(3) Mai, Z. *Membrane processes for water and wastewater treatment: study and modeling of interactions between membrane and organic matter*. Ecole Centrale Paris, 2013.

(4) Tay, M. F.; Liu, C.; Cornelissen, E. R.; Wu, B.; Chong, T. H. The feasibility of nanofiltration membrane bioreactor (NF-MBR)+reverse osmosis (RO) process for water reclamation: Comparison with ultrafiltration membrane bioreactor (UF-MBR)+RO process. *Water Res.* **2018**, *129*, 180–189.

(5) Zhang, X.; Tian, J.; Ren, Z.; Shi, W.; Zhang, Z.; Xu, Y.; Gao, S.; Cui, F. High performance thin-film composite (TFC) forward osmosis (FO) membrane fabricated on novel hydrophilic disulfonated

poly(arylene ether sulfone) multiblock copolymer/polysulfone substrate. *J. Memb. Sci.* **2016**, *520*, 529−539.
(6) Werber, J. R.; Osuji, C. O.; Elimelech, M. Materials for next-generation desalination and water purification membranes. *Nat. Rev. Mater.* **2016**, *1*, 16018.
(7) Zou, S.; Smith, E. D.; Lin, S.; Martin, S. M.; He, Z. Mitigation of bidirectional solute flux in forward osmosis via membrane surface coating of zwitterion functionalized carbon nanotubes. *Environ. Inter.* **2019**, *131*, 104970.
(8) Galiano, F.; Figoli, A.; Deowan, S. A.; Johnson, D.; Altinkaya, S. A.; Veltri, L.; De Luca, G.; Mancuso, R.; Hilal, N.; Gabriele, B.; Hoinkis, J. A step forward to a more efficient wastewater treatment by membrane surface modification via polymerizable bicontinuous microemulsion. *J. Memb. Sci.* **2015**, *482*, 103−114.
(9) Singh, N.; Petrinic, I.; Hélix-Nielsen, C.; Basu, S.; Balakrishnan, M. Concentrating molasses distillery wastewater using biomimetic forward osmosis (FO) membranes. *Water Res.* **2018**, *130*, 271−280.
(10) Habel, J.; Hansen, M.; Kynde, S.; Larsen, N.; Midtgaard, S. R.; Jensen, G. V.; Bomholt, J.; Ogbonna, A.; Almdal, K.; Schulz, A.; Hélix-Nielsen, C. Aquaporin-based biomimetic polymeric membranes: Approaches and challenges. *Membranes (Basel)* **2015**, *5*, 307−351.
(11) Wang, Z.; Wang, X.; Ding, W.; Wang, M.; Qi, X.; Gao, C. Impact of monoolein on aquaporin1-based supported lipid bilayer membranes. *Sci. Tech. Adv. Mater.* **2015**, *16*, 045005−045005.
(12) Ding, W.; Cai, J.; Yu, Z.; Wang, Q.; Xu, Z.; Wang, Z.; Gao, C. Fabrication of an aquaporin-based forward osmosis membrane through covalent bonding of a lipid bilayer to a microporous support. *J. Mater. A Chem. Mater.* **2015**, *3*, 20118−20126.
(13) Pendergast, M. M.; Hoek, E. M. V. A review of water treatment membrane nanotechnologies. *Energ. Environ. Sci.* **2011**, *4*, 1946−1971.
(14) Mauter, M. S.; Elimelech, M.; Osuji, C. O. Nanocomposites of Vertically Aligned Single-Walled Carbon Nanotubes by Magnetic Alignment and Polymerization of a Lyotropic Precursor. *ACS Nano* **2010**, *4*, 6651−6658.
(15) Smith, R. C.; Fischer, W. M.; Gin, D. L. Ordered Poly(p-phenylenevinylene) Matrix Nanocomposites via Lyotropic Liquid-Crystalline Monomers. *J. Am. Chem. Soc.* **1997**, *119*, 4092−4093.
(16) de Souza, J. F.; Pontes, K. D. S.; Alves, T. F. R.; Amaral, V. A.; Rebelo, M. D. A.; Hausen, M. A.; Chaud, M. V. Spotlight on Biomimetic Systems Based on Lyotropic Liquid Crystal. *Molecules* **2017**, *22*, 419.
(17) Astolfi, P.; Giorgini, E.; Gambini, V.; Rossi, B.; Vaccari, L.; Vita, F.; Francescangeli, O.; Marchini, C.; Pisani, M. Lyotropic Liquid-Crystalline Nanosystems as Drug Delivery Agents for 5-Fluorouracil: Structure and Cytotoxicity. *Langmuir* **2017**, *33*, 12369−12378.
(18) Rajabalaya, R.; Musa, M. N.; Kifli, N.; David, S. R. Oral and transdermal drug delivery systems: role of lipid-based lyotropic liquid crystals. *Drug. Des. Devel. Ther.* **2017**, *Volume11*, 393−406.
(19) Bridges, C. R.; Ford, M. J.; Popere, B. C.; Bazan, G. C.; Segalman, R. A. Formation and Structure of Lyotropic Liquid Crystalline Mesophases in Donor−Acceptor Semiconducting Polymers. *Macromolecules* **2016**, *49*, 7220−7229.
(20) Kim, B.-G.; Jeong, E. J.; Chung, J. W.; Seo, S.; Koo, B.; Kim, J. A molecular design principle of lyotropic liquid-crystalline conjugated polymers with directed alignment capability for plastic electronics. *Nat. Mater.* **2013**, *12*, 659−664.
(21) Kerr, R. L.; Miller, S. A.; Shoemaker, R. K.; Elliott, B. J.; Gin, D. L. New Type of Li Ion Conductor with 3D Interconnected Nanopores via Polymerization of a Liquid Organic Electrolyte-Filled Lyotropic Liquid-Crystal Assembly. *J. Am. Chem. Soc.* **2009**, *131*, 15972−15973.
(22) Zhai, J.; Fong, C.; Tran, N.; Drummond, C. J. Non-Lamellar Lyotropic Liquid Crystalline Lipid Nanoparticles for the Next Generation of Nanomedicine. *ACS Nano* **2019**, *13*, 6178−6206.
(23) Carter, B. M.; Wiesenauer, B. R.; Hatakeyama, E. S.; Barton, J. L.; Noble, R. D.; Gin, D. L. Glycerol-Based Bicontinuous Cubic Lyotropic Liquid Crystal Monomer System for the Fabrication of Thin-Film Membranes with Uniform Nanopores. *Chem. Mater.* **2012**, *24*, 4005−4007.
(24) Negrini, R.; Mezzenga, R. pH-Responsive Lyotropic Liquid Crystals for Controlled Drug Delivery. *Langmuir* **2011**, *27*, 5296−5303.
(25) Wang, G.; Garvey, C. J.; Zhao, H.; Huang, K.; Kong, L. Toward the Fabrication of Advanced Nanofiltration Membranes by Controlling Morphologies and Mesochannel Orientations of Hexagonal Lyotropic Liquid Crystals. *Membranes (Basel)* **2017**, *7*, 37.
(26) Zhai, J.; Tran, N.; Sarkar, S.; Fong, C.; Mulet, X.; Drummond, C. J. Self-assembled Lyotropic Liquid Crystalline Phase Behavior of Monoolein−Capric Acid−Phospholipid Nanoparticulate Systems. *Langmuir* **2017**, *33*, 2571−2580.
(27) Kulkarni, C. V.; Wachter, W.; Iglesias-Salto, G.; Engelskirchen, S.; Ahualli, S. Monoolein: a magic lipid? *Phys. Chem. Chem. Phys.* **2011**, *13*, 3004−3021.
(28) Yaseen, M.; Lu, J. R.; Webster, J. R. P.; Penfold, J. The Structure of Zwitterionic Phosphocholine Surfactant Monolayers. *Langmuir* **2006**, *22*, 5825−5832.
(29) Szlezak, M.; Nieciecka, D.; Joniec, A.; Pękała, M.; Gorecka, E.; Emo, M.; Stébé, M. J.; Krysiński, P.; Bilewicz, R. Monoolein cubic phase gels and cubosomes doped with magnetic nanoparticles-hybrid materials for controlled drug release. *ACS Appl. Mater. Inter.* **2017**, *9*, 2796−2805.
(30) Rahanyan-Kagi, N.; Aleandri, S.; Speziale, C.; Mezzenga, R.; Landau, E. M. Stimuli-responsive lipidic cubic phase: Triggered release and sequestration of guest molecules. *Chem. Eur. J.* **2015**, *21*, 1873−1877.
(31) Henmi, M.; Nakatsuji, K.; Ichikawa, T.; Tomioka, H.; Sakamoto, T.; Yoshio, M.; Kato, T. Self-Organized Liquid-Crystalline Nanostructured Membranes for Water Treatment: Selective Permeation of Ions. *Adv. Mater.* **2012**, *24*, 2238−2241.
(32) Nada, H.; Sakamoto, T.; Henmi, M.; Ogawa, T.; Kimura, M.; Kato, T. Transport mechanisms of water molecules and ions in sub-nano channels of nanostructured water treatment liquid-crystalline membranes: a molecular dynamics simulation study. *Environ. Sci. Water Res. Tech.* **2020**, *6*, 604−611.
(33) Hamaguchi, K.; Kuo, D.; Liu, M.; Sakamoto, T.; Yoshio, M.; Katayama, H.; Kato, T. Nanostructured Virus Filtration Membranes Based on Two-Component Columnar Liquid Crystals. *ACS Macro. Lett.* **2019**, *8*, 24−30.
(34) Zhou, S.; Liu, F.; Wang, J.; Lin, H.; Han, Q.; Zhao, S.; Tang, C. Y. Janus Membrane with Unparalleled Forward Osmosis Performance. *Environ. Sci. Tech. Lett.* **2019**, *6*, 79−85.
(35) Yang, H.-C.; Hou, J.; Chen, V.; Xu, Z.-K. Janus Membranes: Exploring Duality for Advanced Separation. *Angew. Chem. Inter. Ed. Engl.* **2016**, *55*, 13398−13407.
(36) Li, C.; Li, X.; Du, X.; Tong, T.; Cath, T. Y.; Lee, J. Antiwetting and Antifouling Janus Membrane for Desalination of Saline Oily Wastewater by Membrane Distillation. *ACS Appl. Mater. Interface* **2019**, *11*, 18456−18465.
(37) Yan, W.; Miao, D.; Babar, A. A.; Zhao, J.; Jia, Y.; Ding, B.; Wang, X. Multi-scaled interconnected inter- and intra-fiber porous janus membranes for enhanced directional moisture transport. *J. Collid Interface Sci.* **2020**, *565*, 426−435.
(38) Clogston, J.; Caffrey, M. Controlling release from the lipidic cubic phase. Amino acids, peptides, proteins and nucleic acids. *J. Control Release* **2005**, *107*, 97−111.
(39) Qiu, H.; Caffrey, M. The phase diagram of the monoolein/water system: metastability and equilibrium aspects. *Biomaterials* **2000**, *21*, 223−234.
(40) Chong, J. Y. T.; Mulet, X.; Waddington, L. J.; Boyd, B. J.; Drummond, C. J. High-Throughput Discovery of Novel Steric Stabilizers for Cubic Lyotropic Liquid Crystal Nanoparticle Dispersions. *Langmuir* **2012**, *28*, 9223−9232.
(41) Fang, Y.; Bian, L.; Bi, Q.; Li, Q.; Wang, X. Evaluation of the pore size distribution of a forward osmosis membrane in three different ways. *J. Memb. Sci.* **2014**, *454*, 390−397.
(42) Huang, X.; Wang, W.; Liu, Y.; Wang, H.; Zhang, Z.; Fan, W.; Li, L. Treatment of oily waste water by PVP grafted PVDF ultrafiltration membranes. *Chem. Eng. J.* **2015**, *273*, 421−429.

https://dx.doi.org/10.1021/acsomega.0c00946
ACS Omega 2020, 5, 17940−17946

(43) Shang, R.; Goulas, A.; Tang, C. Y.; de Frias Serra, X.; Rietveld, L. C.; Heijman, S. G. J. Atmospheric pressure atomic layer deposition for tight ceramic nanofiltration membranes: Synthesis and application in water purification. *J. Memb. Sci.* **2017**, *528*, 163−170.
(44) Liu, T.-Y.; Yuan, H.-G.; Li, Q.; Tang, Y.-H.; Zhang, Q.; Qian, W.; Van der Bruggen, B.; Wang, X. Ion-Responsive Channels of Zwitterion-Carbon Nanotube Membrane for Rapid Water Permeation and Ultrahigh Mono−/Multivalent Ion Selectivity. *ACS Nano* **2015**, *9*, 7488−7496.
(45) Santiago, C. *La fisisorción de nitrógeno. Fundamentos fisicos, normativa, descripción del equipo y procedimiento experimental*; Ministerio de Fomento: Centro de estudios y experimetación de Obras Públicas, 2012; p 96.
(46) Yildirim, Z. E.; Ilis, G. G.; Mobedi, M.; Ülkü, S. Effect of Isotherm Shape on Mass Transfer in an Adsorbent Particle; An Isothermal Adsorption Process. *Open Transp. Phenom. J.* **2011**, *3*, 40−48.
(47) Richardson, S. J.; Staniec, P. A.; Newby, G. E.; Terrill, N. J.; Elliott, J. M.; Squires, A. M.; Góźdź, W. T. Predicting the Orientation of Lipid Cubic Phase Films. *Langmuir* **2014**, *30*, 13510−13515.
(48) Ghosh, S.; Ramos, L.; Remita, H. Swollen hexagonal liquid crystals as smart nanoreactors: implementation in materials chemistry for energy applications. *Nanoscale* **2018**, *10*, 5793−5819.
(49) Gin, D. L.; Gu, W.; Pindzola, B. A.; Zhou, W.-J. Polymerized Lyotropic Liquid Crystal Assemblies for Materials Applications. *Acc. Chem. Res.* **2001**, *34*, 973−980.
(50) Han, Y.; Zhang, D.; Chng, L. L.; Sun, J.; Zhao, L.; Zou, X.; Ying, J. Y. A tri-continuous mesoporous material with a silica pore wall following a hexagonal minimal surface. *Nat. Chem.* **2009**, *1*, 123−127.
(51) Stark, H.; Fukuda, J.-I.; Yokoyama, H. Capillary Condensation in Liquid-Crystal Colloids. *Phys. Rev. Lett.* **2004**, *92*, 205502.
(52) Ravikovitch, P. I.; Neimark, A. V. Density Functional Theory of Adsorption in Spherical Cavities and Pore Size Characterization of Templated Nanoporous Silicas with Cubic and Three-Dimensional Hexagonal Structures. *Langmuir* **2002**, *18*, 1550−1560.
(53) El-Safty, S. A.; Evansb, J. Formation of highly ordered mesoporous silica materials adopting lyotropic liquid crystal mesophases. *J. Mater. Chem.* **2002**, *12*, 117−123.
(54) Puguan, J. M. C.; Kim, H.-S.; Lee, K.-J.; Kim, H. Low internal concentration polarization in forward osmosis membranes with hydrophilic crosslinked PVA nanofibers as porous support layer. *Desalination* **2014**, *336*, 24−31.
(55) Cruz-Tato, P.; Rivera-Fuentes, N.; Flynn, M.; Nicolau, E. Anti-Fouling Electroconductive Forward Osmosis Membranes: Electrochemical and Chemical Properties. *ACS Appl. Polym. Mater.* **2019**, *1*, 1061−1070.
(56) Yu, L.; Zhang, Y.; Wang, Y.; Zhang, H.; Liu, J. High flux, positively charged loose nanofiltration membrane by blending with poly (ionic liquid) brushes grafted silica spheres. *J. Hazard. Mater.* **2015**, *287*, 373−383.
(57) Ray, S. S.; Lee, H. K.; Kwon, Y.-N. Review on Blueprint of Designing Anti-Wetting Polymeric Membrane Surfaces for Enhanced Membrane Distillation Performance. *Polymers (Basel)* **2019**, *12*, 23.
(58) Kolasińska, M.; Warszyński, P. The effect of nature of polyions and treatment after deposition on wetting characteristics of polyelectrolyte multilayers. *Appl. Surf. Sci.* **2005**, *252*, 759−765.
(59) Zou, S.; He, Z. Electrodialysis recovery of reverse-fluxed fertilizer draw solute during forward osmosis water treatment. *Chem. Eng. J.* **2017**, *330*, 550−558.

https://dx.doi.org/10.1021/acsomega.0c00946
ACS Omega 2020, 5, 17940−17946